Optics Letters

Generation of deep ultraviolet sub-2-fs pulses

Mara Galli,[1,2,3,*] Vincent Wanie,[1,4] Diogo Pereira Lopes,[2] Erik P. Månsson,[1] Andrea Trabattoni,[1] Lorenzo Colaizzi,[1] Krishna Saraswathula,[1] Andrea Cartella,[5] Fabio Frassetto,[6] Luca Poletto,[6] François Légaré,[4] Salvatore Stagira,[2,3] Mauro Nisoli,[2,3] Rebeca Martínez Vázquez,[3] Roberto Osellame,[3] and Francesca Calegari[1,3,5,7]

[1]Center for Free-Electron Laser Science (CFEL), DESY, 85 Notkestraße, Hamburg, 22607, Germany
[2]Physics Department, Politecnico di Milano, 32 Piazza Leonardo da Vinci, Milano 20133, Italy
[3]Institute for Photonics and Nanotechnologies, IFN-CNR, 32 Piazza Leonardo da Vinci, Milano 20133, Italy
[4]Institut National de la Recherche Scientifique, Centre Énergie Matériaux et Télécommunications, 1650 Blvd. Lionel-Boulet, Varennes, Québec J3X1S2, Canada
[5]The Hamburg Centre for Ultrafast Imaging, Universität Hamburg, 149 Luruper Chaussee, Hamburg 22761, Germany
[6]Institute for Photonics and Nanotechnologies, IFN-CNR, 7 Via Trasea, Padova 35131, Italy
[7]Department of Physics, Hamburg Universität, 9-11 Jungiusstraße, Hamburg 20355, Germany
*Corresponding author: mara.galli@desy.de

Received 7 January 2019; revised 10 February 2019; accepted 11 February 2019; posted 11 February 2019 (Doc. ID 357022); published 5 March 2019

We demonstrate the generation of few-cycle deep ultraviolet pulses via frequency upconversion of 5-fs near-infrared pulses in argon using a laser-fabricated gas cell. The measured spectrum extends from 210 to 340 nm, corresponding to a transform-limited pulse duration of 1.45 fs. We extract from a dispersion-free second-order cross-correlation measurement a pulse duration of 1.9 fs, defining a new record in the deep ultraviolet spectral range.

https://doi.org/10.1364/OL.44.001308

Absorption of ultraviolet (UV) radiation is associated with electronic excitation. In most of the molecules, this excess of energy is often dissipated via nonradiative decay. Upon UV excitation, ultrafast conversion of electronic energy into vibrational modes has been demonstrated to be at the core of fundamental processes such as DNA damage and photoprotection [1,2]. Owing to the natural temporal scale of electron motion, getting access to these ultrafast mechanisms requires extremely short laser pulses, such as the ones provided by femtosecond or even attosecond laser sources. Nowadays, attosecond science is able to provide subfemtosecond laser pulses with a tunable spectrum over an extremely broad range, from the vacuum UV (VUV) [3] or extreme UV (XUV) [4–6] to the soft x rays [7]. Recently, even subfemtosecond visible (VIS) pulses have been generated [8]. At the same time, few-fs pulses in the visible or near-infrared (NIR) spectral range can be routinely generated via hollow-core fiber compression [9] and filamentation [10]. Nevertheless, the generation of few-fs deep UV (200 to 300 nm) pulses is still extremely challenging. The hurdle arises from the need to optimize a nonlinear optical process over a broad spectral range where compression and phase control are currently not available. In the last two decades, many different techniques have been tested to generate ultrashort UV pulses, such as frequency upconversion [11], optical parametric amplification [12], four-wave mixing [13], or self-phase modulation in hollow-core [14] and photonic crystal fibers [15,16]. Starting from NIR pulses, third harmonic generation (THG) is the most suitable process to be exploited for UV generation. Despite the high conversion efficiency nonlinear crystals can provide, they strongly limit the lowest duration of the upconverted pulses because of intrinsic dispersion and phase-matching constraints [17]. A valid alternative is to use a noble gas as a nonlinear medium for THG [18,19]. This method allows a broad spectral bandwidth to be upconverted without inducing significant dispersion to the generated UV pulses, at the expenses of a lower conversion efficiency. Using this technique, the generation of sub-3-fs pulses has been achieved [18].

In this Letter, we report the generation of 1.9-fs UV pulses centered at 260 nm using THG driven by few-fs NIR pulses in a high-pressure gas cell specifically designed to optimize the process. A pulse energy of 150 nJ was measured on target. To our knowledge, these are the shortest pulses ever generated in the deep UV spectral range, opening up new perspectives for resolving the UV-photoactivated molecular processes at the time scale of electronic motion.

As schematically shown in Fig. 1, 5-fs waveform-controlled NIR pulses (carrier wavelength of 770 nm) are used to seed an interferometric setup: a portion of the NIR beam (250 μJ) is driving the UV generation process, while the remaining part of the NIR beam is either used to temporally characterize the UV radiation via cross-correlation or to generate XUV attosecond pulses. The whole setup is kept under vacuum to avoid dispersion of the UV pulses.

The NIR beam used to generate the UV radiation is focused with an 800-mm focal-length silver mirror into a gas cell filled

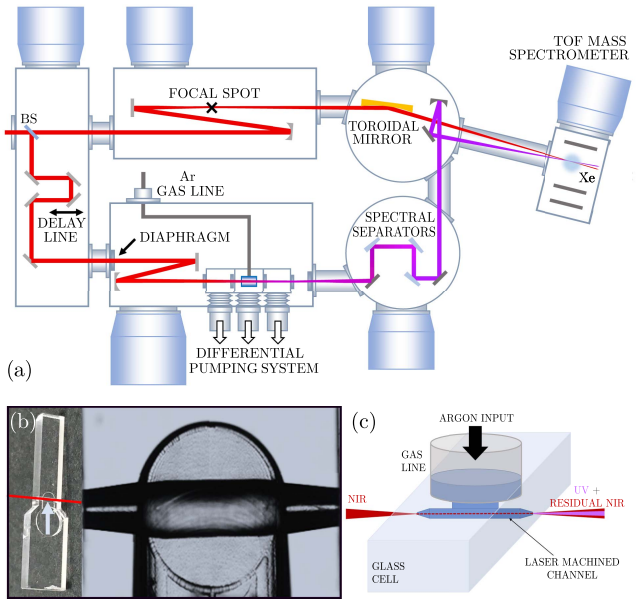

Fig. 1. (a) Experimental setup used for generation and characterization of the sub-2-fs deep UV pulses. (b) Picture of the glass cell used to generate the UV pulses (the red line represents the laser propagation direction, while the light arrow represents the gas flow) and a magnified image of the channel acquired with a microscope. (c) Schematic representation of the gas cell showing the laser beam, the gas inlet, and the channel shape.

with argon where the THG process is induced. The beam waist of the NIR pulse in the interaction point is estimated to be 50 ± 5 μm, with a peak intensity in the range of 1 to $5 \cdot 10^{14}$ W/cm^2. The gas cell has been fabricated in a fused silica slab using femtosecond laser irradiation followed by chemical etching (FLICE) [20,21], and it has been interfaced to a 3-mm metallic tube supplying the gas. The gas cell, shown in panels b and c of Fig. 1, is designed to have a 1-mm-diameter channel in the central section, acting as a reservoir, which is then progressively reduced at the extremities down to 400 μm. The size of the holes has been chosen to fit that of the laser beam and to minimize the outflowing gas. This approach allows the UV generation to be confined within a few millimeters and the phase matching to be optimized. Channel lengths ranging from 3 to 5 mm have been tested to maximize the UV generation. The use of a laser-machined fused silica cell presents several advantages with respect to a conventional metallic one: (1) the channel length and the hole size can be arbitrarily set with extremely high precision (few μm); (2) contrary to metals, glass offers a high transmittance for VIS–NIR radiation, preventing the cell to be damaged by the impinging laser beam (with peak intensities in the order of 10^{14} W/cm^2); and (3) the reservoir can be realized with any arbitrary geometry including guiding channels to further optimize the generation process. This design allows for efficient pumping, which is further improved by inserting the gas cell in a small chamber composed by three differentially pumped sections. This system allows a residual gas pressure of 10^{-3} mbar to be achieved in the main chamber even when operating the setup with several bars of gas in the generation cell. A gas recirculation system has also been implemented to compensate for the high argon consumption. Two sealed pumps are used to pump, respectively, the main vacuum chamber and the three sections of the differential pumping system. In this way, the recirculation of almost the entire gas volume is ensured. The pump exhaust lines are connected to a diaphragm pump, which compresses the gas in a tank up to 7 bars. The gas is then sent back to the UV generation cell through a metallic gas line, where a valve allows for the fine tuning of the pressure at the generation point.

The suppression of the copropagating fundamental NIR component after the UV generation is performed by three dichroic wedged beam separators (LAYERTEC GmbH). They have been installed in the UV optical path in order to transmit most of the NIR spectrum and reflect wavelengths below 350 nm. Attenuation of the NIR pulse energy by 4 orders of magnitude (residual energy 28 nJ) is achieved while preserving more than 85% of the UV pulse energy. In contrast to silicon wafers at Brewster's angle used in previous setups [18], the reflectivity of the separators in the deep UV spectral region is higher than 85% for both s-polarized and p-polarized laser beams, thus allowing for both linear and circular UV radiation to be reflected. In this specific case, the generated UV radiation was linearly polarized. The generated UV pulses can be extracted before reaching the experimental region through a 300-μm-thick UV-grade antireflection coated fused-silica window to characterize both spectrum and energy in air. In Fig. 2(a) we compare the UV spectra obtained for THG in 0.2 bar (yellow solid line) and 1.1 bar (red solid line) of argon gas, respectively. The Fourier transforms of the two spectra are reported in the inset of the figure as black dots. A Gaussian fitting function is used to calculate the transform limited (TL)

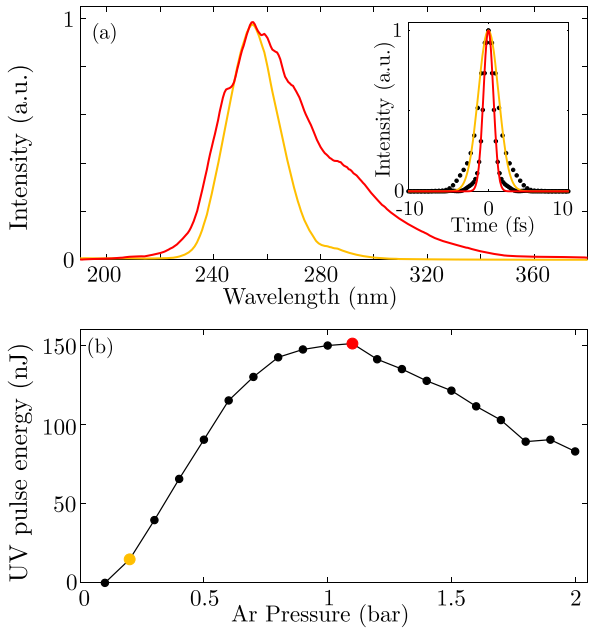

Fig. 2. (a) Spectral intensity profile of the UV pulses acquired for 0.2 bar (yellow solid line) and 1.1 bar (red solid line) of argon. The inset shows the corresponding Fourier transforms (black dots) and the Gaussian fitting functions (solid lines, same color code as the main panel). (b) UV pulse energy measured as a function of the gas pressure. The red dot and the yellow dot correspond to the gas pressure values used for generating the red spectra and yellow spectra reported in (a), respectively.

pulse durations, represented in yellow and red, respectively. The narrowest spectrum corresponds to a TL duration of 3 fs (FWHM), as expected by considering a pure THG process driven by 5-fs NIR pulses, as measured in Ref. [18]. Increasing the gas pressure above 1 bar leads instead to a remarkable spectral broadening of the UV pulse, corresponding to a TL duration of 1.45 fs (FWHM) and indicating the presence of other nonlinear effects. This spectral broadening can only be explained if we take into account pulse reshaping due to nonlinear effects for both the NIR driving pulses and the UV pulses. In particular, Kerr-effect-induced self-phase modulation as well as plasma phase modulation are expected to be the dominant effects. Ionization-induced spectral reshaping in THG has been previously investigated in neon at high gas pressures (>7 bar) [22]. Owing to the lower ionization potential and the remarkably larger χ^3, an even more pronounced effect is expected to occur in argon at much lower gas pressures. As demonstrated in Ref. [22], the ionization-induced self-defocusing occurring on the trailing edge of the driving pulse allows for a tight confinement of the nonlinear processes (including THG) to the leading edge of the pulse itself. This confinement can be interpreted as a gating effect on the THG process, thus resulting in the generation of a UV supercontinuum with a TL close to 1 fs. As shown in Ref. [22], the generated UV continuum is expected to experience a broadening on both sides of the spectrum while propagating in the gas target. It is worth noting that in our experimental conditions, the spectral broadening on the blue side, which also contains a strong contribution from fifth harmonic generation and a cascading of four-wave-mixing processes, cannot be detected due to the limited reflectivity of the optical setup in this spectral region.

Figure 2(b) shows the UV pulse energy as a function of the gas pressure at the generation cell. The maximum efficiency is achieved with 1.1 bar of argon. In this condition the pulse energy on target is around 150 nJ, which, considering the reflectivity of all the optics in the beam path, corresponds to more than 215 nJ at the source (pulse energy stability over several hours within 10%). Higher pressures lead to a reduction of the UV intensity due to strong ionization resulting from plasma-induced defocusing of the NIR beam accompanied by a deterioration of the spatial quality of the UV beam. In the interaction region, the UV pulses are noncollinearly recombined with XUV or NIR pulses. The estimated angle between the two beams is around 7 mrad. Given the photon energy and the spectral extension of our UV radiation, we could not rely on fully optical techniques to temporally characterize the pulses. For this reason, the temporal characterization of the UV pulses has been performed via UV-NIR cross-correlation in xenon [18,23]. The generation yield of the cation Xe^+ has been measured with a time-of-flight mass spectrometer as a function of the relative delay between the NIR and the UV pulses. The tight-angle noncollinear geometry has a small impact on the measured cross-correlation signal, i.e., the retrieved time duration of the UV pulses is 2% longer than for collinear geometry. Figure 3(a) shows the acquired cross-correlation signal: here, for negative delays the UV pulse precedes the NIR pulse. In our measurements, the relative delay was varied with 0.4-fs steps by a piezoelectric delay line.

While performing the cross-correlation measurement, the peak intensity of both the UV and the NIR pulses was checked to be low enough in order to prevent direct multiphoton ionization from each individual pulse. Therefore, ionization of

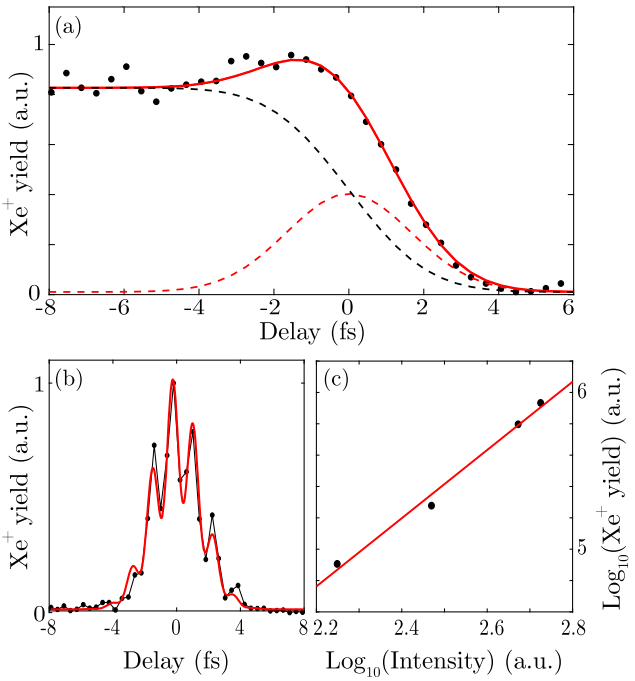

Fig. 3. (a) UV-NIR cross-correlation signal acquired in xenon (black dots). The dashed lines represent the delay-dependent response of the two open ionization channels: (i) simultaneous absorption of 2 UV + 2 NIR photons (red dashed line) and (ii) resonance-enhanced transition (black dashed line). The red solid line corresponds to the sum of the two contributions. (b) Auto-correlation signal of the NIR pulses acquired in xenon (black line and dots) and auto-correlation fitting function (red solid line). (c) Scaling (black dots) of the peak cross-correlation signal as a function of the NIR intensity in bilogarithmic scale. The red solid line represents the linear function used to fit the data.

xenon ($I_p = 12.13$ eV) could result only from the combination of the two pulses. This constraint, together with the absorption cross-sections of xenon [24,25], allowed us to narrow down the set of possible nonlinear processes leading to ionization, i.e. either 1 or 2 UV photons combined with 5 or 2 NIR photons, respectively. The cross-correlation signal has been measured for different NIR intensities to disclose the number of NIR photons involved in the ionization process. The resulting intensity scaling is shown in Fig. 3(c) in bilogarithmic scale. The linear fitting function $y = mx + q$ used to fit the data has a slope coefficient $m = 2.176 \pm 0.354$. This result is thus indicating a second-order nonlinear process, demonstrating that the proposed cross-correlation scheme is involving 2 UV and 2 NIR photons. The experimental cross-correlation signal [black dots in Fig. 3(a)] exhibits an overall steplike dynamics that has to be analyzed taking into account the electron energy structure of xenon. In fact, the acquired dynamics can be attributed to a sum of two different ionization channels. A simultaneous transition is occurring when the two pulses are temporally overlapped and 2 UV + 2 NIR photons are absorbed at the same time, leading to direct xenon ionization and thus giving rise to a Gaussian contribution in the dynamics [red dashed line in Fig. 3(a)]. A resonance-enhanced sequential transition inducing xenon ionization is also occurring, and it involves a xenon long-lived electronically excited state accessible only after the absorption of 2 UV photons. Considering the UV second-order

contribution and the dipole selection rules for the optical transition, the only possible metastable state responsible for the sequential ionization transition is the $5p_5 6p$ state. The energy of this state (fine structure between 9.5 and 10 eV) is indeed compatible with the absorption of 2 UV photons, which can lead to ionization when followed by absorption of 2 NIR photons [26]. The sequential resonance-enhanced transition is described by an error function contribution to the overall dynamics, which is represented by the black dashed line in Fig. 3(a). For this reason, the cross-correlation dynamics has been fitted with the function $f(t)$ defined as a sum of a Gaussian function and an error function taking into account the direct and the sequential ionization transitions, respectively:

$$f(t) = A_1 \exp(-(t - t_0)^2/2\sigma^2) + A_2 \operatorname{erf}\left((t - t_0)/\sqrt{2}\sigma\right). \tag{1}$$

The time offset t_0 and the width σ have been kept the same for the two contributions, while the relative amplitudes A_1 and A_2 have been left as free parameters. The time offset corresponds to the temporal overlap between the UV and NIR pulses, while the parameter σ has been used to retrieve the UV pulse duration as shown in Eq. (2) ($\mathrm{FWHM}_{\mathrm{UV}} = 2.355\sigma_{\mathrm{UV}}$):

$$\sigma = \sqrt{\sigma_{\mathrm{UV}}^2/n_{\mathrm{UV}} + \sigma_{\mathrm{NIR}}^2/n_{\mathrm{NIR}}}. \tag{2}$$

Here n_{UV} and n_{NIR} represent the number of UV and NIR photons involved in the cross-correlation process, respectively. The cross-correlation fitting function [$f(t)$ in Eq. (1)] is represented by the red solid line in Fig. 3(a). Furthermore, oscillations at twice the frequency of the laser fundamental are visible on top of the cross-correlation dynamics, mainly for negative time delays. These can be attributed to interference between the residual NIR photons reflected by the separators in the UV arm and the NIR beam. To extract the time duration of the UV pulses from the cross-correlation measurement, an independent temporal characterization of the NIR pulse duration is required. This was done by means of an autocorrelation measurement in xenon, performed by replacing the spectral separators with silver mirrors and removing the gas from the UV generation cell. This allowed the combining of two replicas of the NIR pulses in the interaction region, each contributing to xenon ionization with 4 photons. Figure 3(b) reports both the experimental data (black line and dots) and the fitting function (red line). From the fit we retrieved a NIR pulse duration of 5.2 ± 0.2 fs (FWHM).

By inserting the retrieved NIR pulse duration in Eq. (2), we extracted a UV pulse duration of 1.9 ± 0.4 fs (FWHM). The measured UV pulse duration is very close to the transform limit, thus indicating that our generation scheme is almost dispersion free.

In conclusion, we have demonstrated the generation of sub-2-fs deep UV pulses with a 150 nJ energy per pulse. A key aspect of our scheme is the use of a laser microfabricated gas cell allowing for the optimization of gas pressure and generation geometry. Further optimization of the UV generation process could be achieved by replacing the reservoir geometry with an integrated guiding channel [27]. These ultrashort UV pulses can be combined with few-fs NIR pulses or XUV attosecond pulses for time-resolved experiments. Our scheme opens new and important perspectives for investigating ultrafast processes at the electron time scale in UV-excited biochemically relevant molecules.

Funding. H2020 European Research Council (ERC) (637756); Fonds de recherche du Québec—Nature et technologies (FRQNT); National Science and Engineering Research Council (SERC); Vanier Canada Graduate Scholarship (Vanier CGS); Deutsche Forschungsgemeinschaft (DFG) (390715994).

REFERENCES

1. T. Gustavsson, R. Improta, and D. Markovitsi, J. Phys. Chem. Lett. **1**, 2025 (2010).
2. C. E. Crespo-Hernandez, B. Cohen, and B. Kohler, Nature **436**, 1141 (2005).
3. D. Fabris, T. Witting, W. A. Okell, D. J. Walke, P. Matia-Hernando, J. Henkel, T. R. Barillot, M. Lein, J. P. Marangos, and J. W. G. Tisch, Nat. Photonics **9**, 383 (2015).
4. G. Sansone, E. Benedetti, F. Calegari, C. Vozzi, L. Avaldi, R. Flammini, L. Poletto, P. Villoresi, C. Altucci, R. Velotta, S. Stagira, S. D. Silvestri, and M. Nisoli, Science **314**, 443 (2006).
5. F. Krausz and M. Ivanov, Rev. Mod. Phys. **81**, 163 (2009).
6. F. Calegari, G. Sansone, S. Stagira, C. Vozzi, and M. Nisoli, J. Phys. B **49**, 062001 (2016).
7. S. L. Cousin, N. D. Palo, B. Buades, S. M. Teichmann, M. Reduzzi, M. Devetta, A. Kheifets, G. Sansone, and J. Biegert, Phys. Rev. X **7**, 041030 (2017).
8. M. T. Hassan, T. T. Luu, A. Moulet, O. Raskazovskaya, P. Zhokhov, M. Garg, N. Karpowicz, A. M. Zheltikov, V. Pervak, and E. G. F. Krausz, Nature **530**, 66 (2016).
9. M. Nisoli, S. D. Silvestri, and O. Svelto, Appl. Phys. Lett. **68**, 2793 (1996).
10. C. P. Hauri, W. Kornelis, F. W. Helbing, A. Heinrich, A. Couairon, A. Mysyrowicz, J. Biegert, and U. Keller, Appl. Phys. B **79**, 673 (2004).
11. P. Baum, S. Lochbrunner, and E. Riedle, Appl. Phys. B **79**, 1027 (2004).
12. P. Tzankov, T. Fiebig, and I. Buchvarov, Appl. Phys. Lett. **82**, 517 (2003).
13. Y. Kida, J. Liu, T. Teramoto, and T. Kobayashi, Opt. Lett. **35**, 1807 (2010).
14. C. G. Durfee, S. Backus, H. C. Kapteyn, and M. M. Murnane, Opt. Lett. **24**, 697 (1999).
15. F. Kottig, F. Tani, C. M. Biersach, J. C. Travers, and P. St.J. Russell, Optica **4**, 1272 (2017).
16. C. Brahms, D. R. Austin, F. Tani, A. S. Johnson, D. Garratt, J. C. Travers, J. W. Tisch, P. St.J. Russell, and J. P. Marangos, Opt. Lett. **44**, 731 (2019).
17. J. Ringling, O. Kittelmann, F. Noack, G. Korn, and J. Squier, Opt. Lett. **18**, 2035 (1993).
18. F. Reiter, U. Graf, M. Schultze, W. Schweinberger, H. Schröder, N. Karpowicz, A. M. Azzeer, R. Kienberger, F. Krausz, and E. Goulielmakis, Opt. Lett. **35**, 2248 (2010).
19. G. H. C. New and J. F. Ward, Phys. Rev. Lett. **19**, 556 (1967).
20. A. Marcinkevičius, S. Juodkazis, M. Watanabe, M. Miwa, S. Matsuo, H. Misawa, and J. Nishii, Opt. Lett. **26**, 277 (2001).
21. K. Vishnubhatla, N. Bellini, R. Ramponi, G. Cerullo, and R. Osellame, Opt. Express **17**, 8685 (2009).
22. F. Reiter, U. Graf, E. E. Serebryannikov, W. Schweinberger, M. Fiess, M. Schultze, A. M. Azzeer, R. Kienberger, F. Krausz, A. M. Zheltikov, and E. Goulielmakis, Phys. Rev. Lett. **105**, 243902 (2010).
23. E. M. Bothschafter, A. Schiffrin, V. S. Yakovlev, A. H. Azzeer, F. Krausz, R. Ernstorfer, and R. Kienberger, Opt. Express **18**, 9173 (2010).
24. L. Allen, D. G. C. Jones, and D. G. Schofield, J. Opt. Soc. Am. **59**, 842 (1969).
25. S. Kröll and W. K. Bischel, Phys. Rev. A **41**, 1340 (1990).
26. A. Schmitt and H. Schmoranzer, Phys. Lett. A **263**, 193 (1999).
27. A. Ciriolo, R. M. Vazquez, G. Crippa, D. Faccialà, M. Negro, M. Devetta, D. Lopes, A. Pusala, C. Vozzi, R. Osellame, and S. Stagira, in *Conference on Lasers and Electro-Optics* (2018).